Ind. J. Pharm. Edu. Res., 2026; 60(1):393-409.
https://www.ijper.org

Original Article

Deciphering Key Protein Targets, Hub Gene Networks, Signaling Pathways and *in silico* Docking Studies of Artemisinin in Human Lung Carcinoma

Xin Sheng[1,#], Dandan Sheng[2,#], Ruiqing Xing[3,*]

[1]Department of Pulmonary and Critical Care Medicine-Section 1, The Second Affiliated Hospital of Chengdu Medical College, Nuclear Industry 416 Hospital, Chengdu Sichuan, CHINA.
[2]Department of Tuberculosis, Yantai Qishan Hospital, Yantai Shandong, CHINA.
[3]Department of Clinical Laboratory Medicine, Xijing Hospital, Fourth Military Medical University, Xi'an Shaanxi, CHINA.
[#]Xin Sheng and Dandan Sheng are co-first authors, they contributed equally to this work.

ABSTRACT

Background: Artemisinin has been reported to exert potent anticancer effects in diverse cancers, but its mode of anticancer action is not fully understood. **Objectives:** This study involved network pharmacology, bioinformatics, *in silico* molecular docking and dynamics along with experimental validation to demonstrate the anticancer activity as well as detailed mode of action of artemisinin in lung cancer. **Materials and Methods:** SwissADME and Protox-II analyzed physicochemical properties and toxicity of artemisinin, while SuperPred and SwissTargetPrediction predicted the biological targets. Lung cancer targets identified from Genecards overlapped with targets of artemisinin using Venny 2.0.2. The intersecting gene targets were submitted to STRING for PPI network development and hub gene identification was done using Cytoscape CytoHubba plugin. ShinyGo platform enabled Gene Ontology and KEGG pathway analysis, whereas UALCAN database revealed DNA methylation, gene expression and survival analysis of hub genes. The correlation between hub gene expression and immune cell infiltration into the tumor microenvironment was studied using the TIMER database. Molecular docking was done using CB-Dock2 and MD simulation with CABS-flex. *In vitro* experimental assays using MTT, fluorescence microscopy (AO/EB staining) and western blotting evaluated the effects of artemisinin on cell viability, apoptosis and hub-gene expression. **Results:** The constructed PPI network comprised 137 nodes and 858 edges, identifying 10 hub genes, including EGFR, HSP90AA1 and PTGS2. Functional analysis revealed significant enrichment in processes like Protein kinase activity and pathways such as PD-L1 expression and PI3K-Akt signalling. UALCAN analyses indicated elevated DNA methylation of EGFR and HSP90AA1, while HSP90AA1 and HSP90AB1 were upregulated in mRNA expression. Immune infiltration analysis showed a positive correlation between hub gene expression and tumor infiltration especially NFKB1 and EGFR. Molecular docking confirmed strong binding affinities of artemisinin to hub genes and molecular dynamics simulations supported stable interactions. Artemisinin demonstrated dose-dependent cytotoxicity in A549 cells, inducing apoptosis and downregulating key hub proteins EGFR, PTGS2 and HSP90AA1 validating the bioinformatics results. **Conclusion:** Our findings highlight the potential of artemisinin as a therapeutic agent in lung cancer, highlighting its targets and associated pathways for further investigation.

Keywords: Apoptosis, Artemisinin, Gene-ontology, Immune infiltration, Lung cancer, Natural products, Network pharmacology.

Correspondence:
Dr. Ruiqing Xing
Department of Clinical Laboratory Medicine, Xijing Hospital, Fourth Military Medical University, Xi'an Shaanxi, CHINA.
Email: ruiqingxing99@hotmail.com
ORCID: 0009-0003-4661-0170

Received: 06-11-2024;
Revised: 18-02-2025;
Accepted: 27-05-2025.

INTRODUCTION

Non-Small Cell Lung Cancer (NSCLC) and Small Cell Lung Cancer (SCLC) are the two main subtypes of lung cancer, which continues to be a major cause of cancer death globally. In 2024, 125,070 cancer deaths and 234,580 new cancer cases were projected to occur in the United States.[1,2] About 85% of cases are NSCLC, which often manifests at an advanced stage since early cancer development is silent.[3] Currently available treatments include immunotherapy, targeted medicines, radiotherapy, chemotherapy and surgery.[4] Some patients have seen better results with targeted therapy, including those that target ROS1 mutations, Anaplastic Lymphoma Kinase (ALK) and the Epidermal Growth Factor Receptor (EGFR).[5,6] To counteract drug resistance and tumor heterogeneity, novel therapeutic

DOI: 10.5530/ijper.20261248

agents and multi-target approaches are necessary since resistance to conventional therapies often arises.

The sweet wormwood plant *Artemisia annua* produces artemisinin, a sesquiterpene lactone that has attracted a lot of interest because of its strong antimalarial attributes, particularly against *Plasmodium falciparum* that are resistant to conventional treatments.[7] In addition to malaria, a variety of diseases, such as cancers, viral infections and parasite disorders, have demonstrated positive therapeutic responses to artemisinin and its derivatives, such as artesunate and artemether.[8] The primary mechanism of artemisinin is associated with its endoperoxide bridge, which generates Reactive Oxygen Species (ROS) by interaction with intracellular iron.[9] The growing potency of Artemisinin as a multi-target therapeutic agent has been demonstrated by its tendency to specifically disrupt cellular processes in certain cancer cells.

Bioinformatics and network pharmacology are transforming drug discovery and development by providing insights into the complex interactions between drugs, targets and disease pathways.[10] Network pharmacology integrates data from various biological networks, such as gene-protein, protein-protein and disease-pathway interactions, allowing researchers to uncover potential targets and predict the therapeutic effects of compounds. Paclitaxel, for instance, has been analyzed using network pharmacology to identify multiple targets across various cancers, elucidating its mechanism of action beyond traditional drug-target interactions.[11] Additionally, network pharmacology allows for the evaluation of synergistic effects, offering a systematic approach to identifying drug combinations that may enhance efficacy and reduce adverse effects.

Tumor growth and treatment resistance in lung cancer are significantly influenced by the Tumor Microenvironment (TME).[12] The effectiveness of immunotherapies has been shown to be impacted by immunological infiltration, which comprises a range of immune cells including T-cells, B-cells, neutrophils and macrophages.[13] Particularly in immunotherapy, the degree and kind of immune cell infiltration are correlated with treatment outcomes and patient prognosis. Bioinformatic tools have become essential in analysing immune cell infiltration patterns, which helps stratify patients likely to benefit from immune checkpoint inhibitors, such as PD-1/PD-L1 inhibitors. Integrating network pharmacology and immune infiltration data can provide a comprehensive understanding of lung cancer pathogenesis, potentially leading to novel therapeutic approaches that harness the immune system while targeting cancer-specific pathways. A Protein-Protein Interaction (PPI) network is a graphical representation of the physical or functional interactions between proteins in a biological system. Each protein is represented as a node and the interactions between them are represented as edges. PPI networks help to elucidate the functional organization and dynamic properties of biological systems, enabling the study of cellular processes and diseases at the molecular level. Hub targets are highly connected proteins within the network (nodes with a high degree of connectivity).

In this study, we utilized bioinformatics and network pharmacology approaches to evaluate the potential of artemisinin in lung cancer. The network-derived insights were integrated with immune infiltration, gene expression and survival analyses. Validation was conducted through molecular docking and dynamic simulations. Furthermore, the combined findings from bioinformatics, network pharmacology, immune infiltration and differential gene expression analyses were corroborated through *in vitro* experimentation. Figure 1 illustrates the flow diagram depicting the workflow for this study.

MATERIALS AND METHODS

Evaluation of physicochemical properties

The physicochemical properties of artemisinin, including drug-likeness, Blood-Brain Barrier (BBB) permeability, solubility and bioavailability, were assessed using SwissADME, a widely used tool for predicting ADME (absorption, distribution, metabolism and excretion) characteristics critical for therapeutic development.[14] Toxicological profiles, including neurotoxicity, hepatotoxicity, cytotoxicity and cardiotoxicity, were evaluated using ProTox-II, providing a comprehensive toxicity analysis for safety profile of artemisinin.

Compound targets and disease targets

Biological targets associated with artemisinin were identified through SuperPred (https://prediction.charite.de/subpages/target_prediction.php) and SwissTargetPrediction (http://www.swisstargetprediction.ch/), two databases that leverage cheminformatics and pharmacophore-based approaches to predict potential molecular targets.[15] The overlapping targets from the two databases were removed and a common compound target file was generated in MS Excel. To investigate lung cancer-specific targets, data was obtained from the GeneCards database, which compiles information on gene-disease associations and relevance to lung cancer pathology. Common targets between artemisinin and lung cancer were identified using Venny 2.0.2, an intersection tool that enables detection of overlapping targets to narrow down relevant molecular interactions.

Network Construction

A Protein-Protein Interaction (PPI) network was constructed for the shared targets using the STRING database (https://string-db.org/), a resource that maps known and predicted interactions to elucidate functional associations among proteins.[16] We employed a medium confidence score>0.4 for considering the PPI interaction as biologically meaningful. The resulting PPI network was visualized in Cytoscape and hub genes, which represent highly connected nodes and potential key targets, were

identified using the CytoHubba plugin. These hub genes provide insight into critical regulatory genes that could serve as potential therapeutic targets within the context of artemisinin and lung cancer. Medium confidence: Scores>0.4

Functional Enrichment

Common genes between lung cancer and artemisinin were analyzed for functional enrichment using the ShinyGO platform (http://bioinformatics.sdstate.edu/go/), which enables Gene Ontology (GO) and KEGG pathway analysis to reveal biological processes, cellular components and pathways associated with the identified targets. ShinyGO provides interactive visualization options, by integrating large annotation database derived from STRING-db and Ensembl into gene function within broader biological contexts.

Differential gene expression, methylation and survival analysis

Hub genes identified in the PPI network were further evaluated for differential expression, survival analysis and gene methylation patterns using the UALCAN portal (https://ualcan.path.uab.edu/).[17] UALCAN ("University of ALabama at Birmingham CANcer data analysis Portal") is an integrative platform that utilizes TCGA data to provide a comprehensive analysis of gene expression profiles, prognostic relevance and methylation status in various cancers.

Immune-infiltration

The immune infiltration status of hub genes was assessed using the TIMER database (http://timer.cistrome.org/), which estimates immune cell infiltration levels, including CD8+ T-cells, CD4+ T-cells, macrophages, B-cells, neutrophils and dendritic cells, in the tumor microenvironment.[18] TIMER offers insights into immune involvement and the potential impact of these cells on disease progression and therapeutic response in lung cancer. TIMER is a user-friendly tool that enables cancer researchers to explore tumor-immune interactions by analysing six types of immune cell infiltration across 32 cancer types, covering 10,897 tumor samples. With six analytic modules, TIMER facilitates investigation of correlations between immune infiltrates, gene expression, clinical outcomes, mutations and copy number changes, making it a valuable resource for dynamic cancer immunology research.

Molecular docking

Molecular docking for hub genes was conducted using the CB-Dock2 online tool (https://cadd.labshare.cn/cb-dock2/index.php), which predicts potential binding sites and facilitates docking with high accuracy.[19] Protein structures were sourced from the RCSB PDB database for EGFR, HSP90AA1 and PTGS2 with PDB IDs 4I23, 1UY6 and 1CX2. The structures were pre-processed in BIOVIA Discovery Studio Visualizer, where water molecules were removed, polar hydrogens were added and crystallized ligands were excluded to ensure readiness for docking. Binding sites on the proteins were identified through CB-Dock2 CurPocket analysis, with the top five predicted pockets docked with artemisinin, whose structure was obtained from the PubChem database. The resulting docked complexes were visualized in Discovery Studio, providing detailed 2D and 3D interaction maps to analyse binding affinities and interactions.

Molecular Dynamic Simulations

CABS-Flex (https://biocomp.chem.uw.edu.pl/CABSflex2/about) was used to simulate protein flexibility and conformational changes in hub gene complexes with artemisinin, offering insights into stability and dynamic properties essential for therapeutic applications.[20] The artemisinin docked to hub genes EGFR, HSP90AA1 and PTGS2 was downloaded from the CB-Dock2 platform in .pdb format and then uploaded to the platform by simulating all the chains present in the complex.

Chemicals, reagents and Cell culture

Artemisinin (98% purity, HPLC) and all other chemicals were purchased from Sigma Aldrich. A549 lung cancer cells (Chinese Academy of Sciences, Shanghai, China) and L132 human embryonic epithelial lung cells (Chinese Academy of Sciences, Shanghai, China) were cultured in Dulbecco's Modified Eagle Medium (DMEM) with 10% FBS and 1% penicillin-streptomycin. Cells were cultured at 37°C in a humidified incubator with 5% CO_2 and the media was changed every 48 hr. At 70-80% confluence, cells were subjected to different concentrations of artemisinin for subsequent experiments.

MTT Assay

The MTT assay assessed cell viability after artemisinin treatment. A549 and L132 cells kept under similar conditions were plated in a 96-well plate at a density of 5×10^3 cells per well and permitted to adhere overnight. Cells were subsequently treated with control, 15, 45, 75 and 150 mg/mL of artemisinin for duration of 24 hr. Following treatment, 20 µL of MTT reagent (5 mg/mL) was introduced to each well and incubated for 4 hr at 37°C. Formazan crystals produced by metabolically active cells were dissolved in 150 µL DMSO and absorbance was recorded at 570 nm using a microplate reader (Thermo Fisher Scientific, Dongcheng District, Beijing, 100013, China). The analysis involved calculating the percentage of viable cells relative to the control group.

Clonogenic Assay

A549 cells were subjected to artemisinin treatment at varying concentrations (control, 15, 75 and 150 mg/mL) for duration of 24 hr. Following treatment, the cells were trypsinized and subsequently plated at low density in 6-well plates to evaluate colony formation. Cells were cultured for duration of 14 days, with media changes occurring every 3 to 4 days. Colonies were fixed

Table 1: Prediction of various physicochemical properties essential for a potential drug candidate using SwissADME, Toxicity was predicted by Pro-Tox 3.0.

Sl. No.	Descriptor	Value
1	Molecular Weight	282.33 g/mol
2	LogP	1.3274
3	Rotatable Bonds	0
4	Hydrogen bond acceptors	5
5	Hydrogen bond donors	0
6	Topological Polar Surface Area (TPSA)	53.99 Å²
7	Water solubility	Soluble
8	Intestinal absorption (human)	High
9	Blood Brain Barrier (BBB) permeability	Yes
10	Bioavailability Score	0.55
11	Druglikeness	Yes, 0 violations from Lipinski rule of 5.
12	Log Kp (skin permeation)	-5.96 cm/s
13	Hepatotoxicity	No
14	Neurotoxicity	No
15	Cytotoxic	No
16	Cardiotoxicity	No

using methanol and stained with crystal violet prior to counting, to assess the impact of artemisinin on the colony-forming capacity of A549 cells.

Acridine Orange/Ethidium Bromide (AO/EB) staining

To evaluate apoptosis in artemisinin-treated A549 cells, researchers used AO/EB staining. Before being treated with 0, 15, 75, or 150 µg/mL artemisinin for 24 hr, cells were spread out in 6-well plates and left to incubate until they reached 70-80% confluency. Cells were rinsed with PBS after treatment and stained using AO/EB solution (100 µg/mL of each dye). Through the use of a fluorescent microscope (Olympus, USA), the stages of cell death were marked: green for healthy cells, bright green for early apoptotic cells with fragmented nuclei and orange/red for late apoptotic or necrotic cells stained with ethidium bromide.

Western blotting

A549 cells were cultured to 80% confluency and treated with artemisinin at 0, 15, 75 and 150 µg/mL. The cells were lysed after 24 hr in RIPA buffer containing protease and phosphatase inhibitors. Protein concentrations were determined by BCA assay and equal amounts of protein were loaded onto SDS-PAGE gels for Western blotting of EGFR, HSP90AA1 and PTGS2 proteins. Following electrophoresis, proteins were transferred to PVDF membranes, blocked with 5% non-fat milk and incubated overnight at 4°C with primary antibodies for EGFR, HSP90AA1, PTGS2 and GAPDH (loading control). After washing, membranes were incubated with HRP-conjugated secondary antibodies, developed using ECL substrate and visualized. The relative expressions of the hub genes were gauged by using ImageJ software.

Statistical analysis

All data are presented as Mean±SD from three independent replicates. Statistical analysis was conducted using GraphPad Prism software, employing Student's *t*-test followed by one-way ANOVA. *p*-values of <0.05, <0.01 and <0.001 were considered statistically significant.

RESULTS

Physicochemical properties

Artemisinin has advantageous physicochemical characteristics that correspond with its beneficial drug-like profile and therapeutic potential (Table 1). Artemisinin has a modest LogP of 1.3274, which optimizes its hydrophilicity and lipophilicity, hence improving cellular absorption and dispersion. The absence of rotatable bonds enhances structural stiffness, possibly increasing receptor binding selectivity. The molecule has five hydrogen bond acceptors and lacks donors, resulting in a Polar Surface Area (TPSA) of 53.99 Å², which facilitates membrane permeability and solubility. Artemisinin, being water-soluble and exhibiting strong intestine absorption, attains effective systemic exposure. Furthermore, it traverses the blood-brain barrier, suggesting possible uses for neurological disorders (Figure 2). A bioavailability score of 0.55 and the absence of Lipinski violations affirm its advantageous drug-likeness, positioning artemisinin as a viable choice for oral administration. Moreover, its safety profile is augmented by the lack of hepatotoxicity, neurotoxicity, cytotoxicity and cardiotoxicity, indicating that artemisinin is well-tolerated and appropriate for therapeutic use.

Network construction

Using SuperPred and SwissTargetPrediction, 147 biological targets were identified for artemisinin (Suppl. Table S1), while 3,697 targets related to lung cancer were obtained from the GeneCards database (Suppl. Table S2). Target intersections were analyzed with Venny 2.0.2, revealing 138 overlapping genes between artemisinin's targets and those implicated in lung cancer (Figure 3A).

These intersecting genes were submitted to the STRING database for PPI network construction, with a minimum confidence level of 0.40 and 3D visualization enabled to enrich network complexity. The resulting .tsv file was downloaded, converted to an MS Excel format and imported into Cytoscape for further analysis and visualization. The constructed PPI network contained 137 nodes and 858 edges, indicating strong interactions with an average

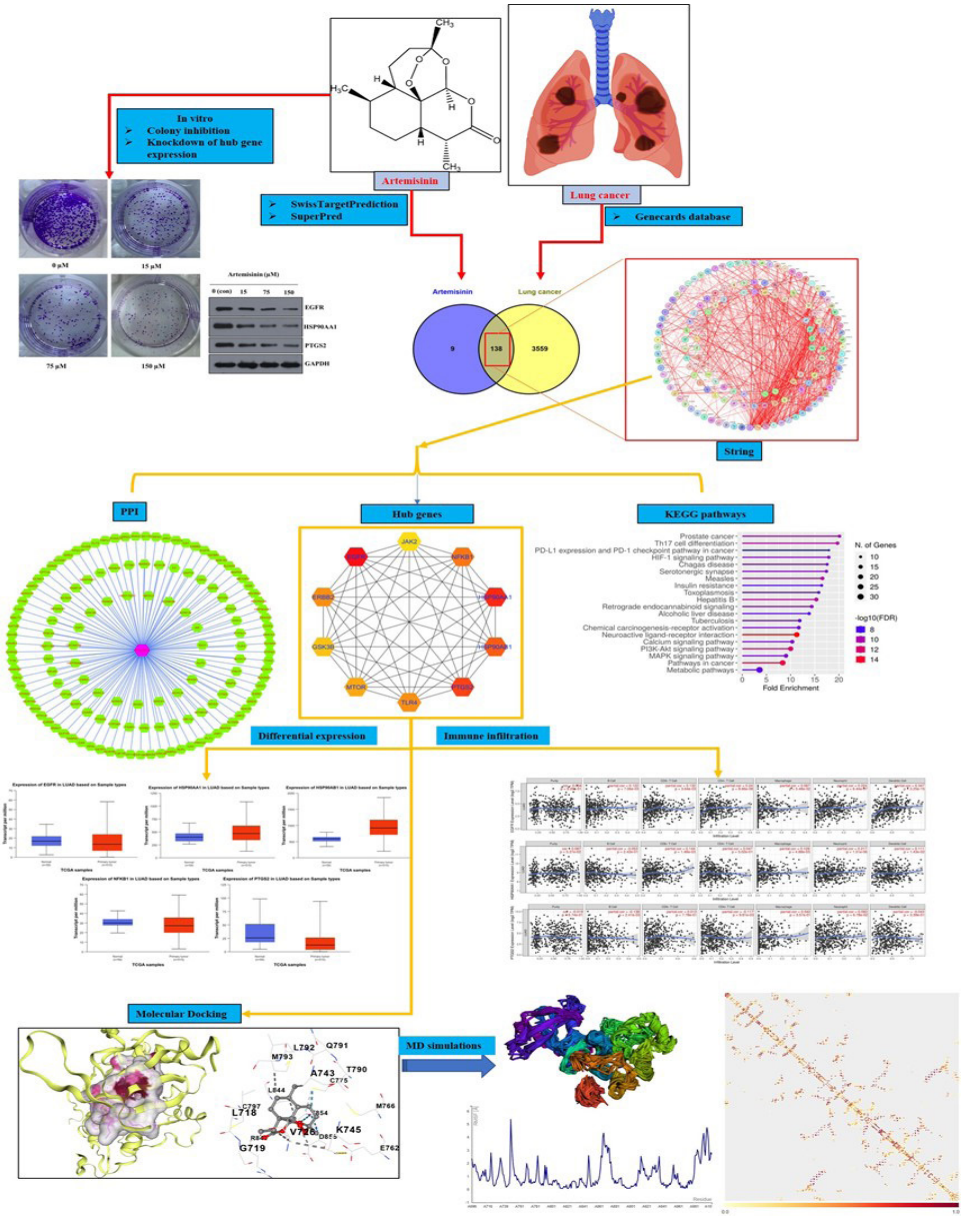

Figure 1: Flow diagram representing the workflow of our study.

neighbour count of 12.526 (Figure 3B). To pinpoint critical gene targets within the network, the CytoHubba plugin in Cytoscape was employed, specifically applying the degree method, which identifies highly connected nodes or "hub genes." Analysis revealed 10 key hub genes, including EGFR, HSP90AA1, PTGS2 and NFKB1 (Figure 3C), known to play significant roles in cancer progression, cell proliferation, inflammation and stress responses.

Functional enrichment analysis

ShinyGO, a compelling web-based tool for functional enrichment analysis for gene sets, was used to analyze common targets. This allows researchers to interactively examine biological processes, molecular activities and cellular components. The BP analysis revealed significant enriched terms such as "Response to organonitrogen compound," "Cellular response to oxygen-containing compound," and "Regulation of cell communication," indicating the targets' involvement in various cellular responses and signaling mechanisms (Figure 4A). In terms of MF, key activities identified included "Protein kinase activity," "ATP binding," and "Transferase activity," emphasizing the importance of phosphorylation and signaling in biological pathways (Figure 4B). The CC analysis identified enriched terms such as "Synaptic membrane," "Dendrite," and "Plasma membrane region," suggesting roles in membrane-associated structures and neuronal signaling (Figure 4C).

Furthermore, KEGG pathway analysis indicated involvement in crucial pathways, including the "PD-L1 expression and PD-1 checkpoint pathway in cancer," "HIF-1 signaling pathway," and "PI3K-Akt signaling pathway" (Figure 4D) This comprehensive analysis highlights the potential of artemisinin targets in regulating

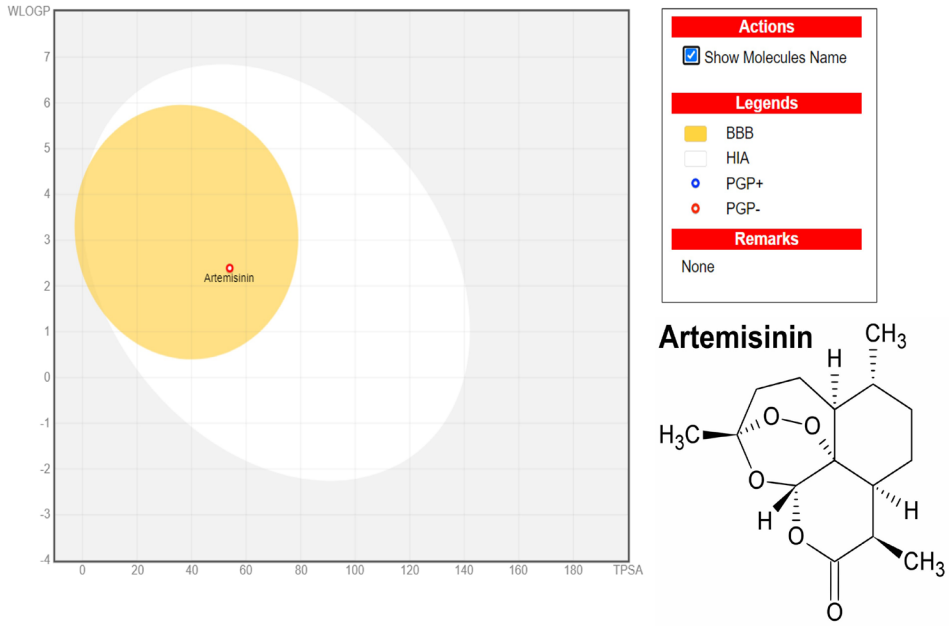

Figure 2: The SwissADME generated boiled egg model for the physiochemical properties of artemisinin. The presence of artemisinin inside the yellow yolk reveals its high blood brain barrier permeability.

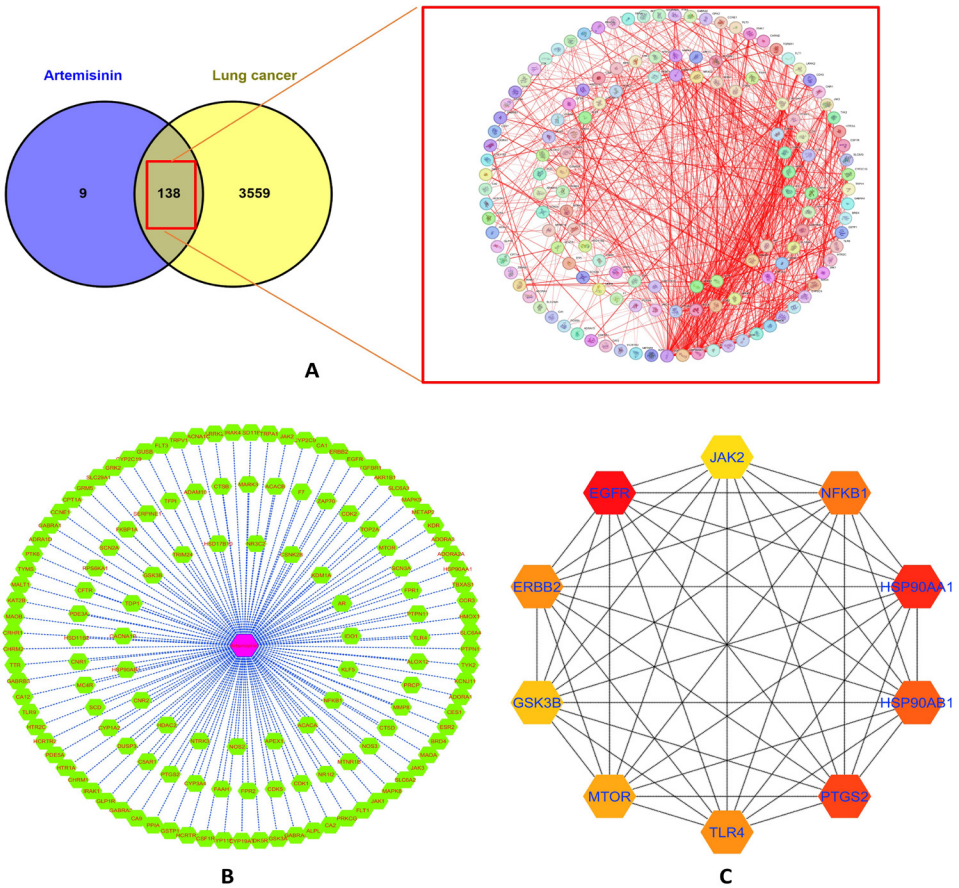

Figure 3: (A) Venn analysis identified 138 overlapping targets between artemisinin and lung cancer. (B) These genes were used to construct a PPI network via STRING with 137 nodes and 858 edges, visualized in Cytoscape. (C) Hub gene analysis with CytoHubba highlighted 10 key genes (Figure 2C), including EGFR, HSP90AA1, PTGS2 and NFKB1.

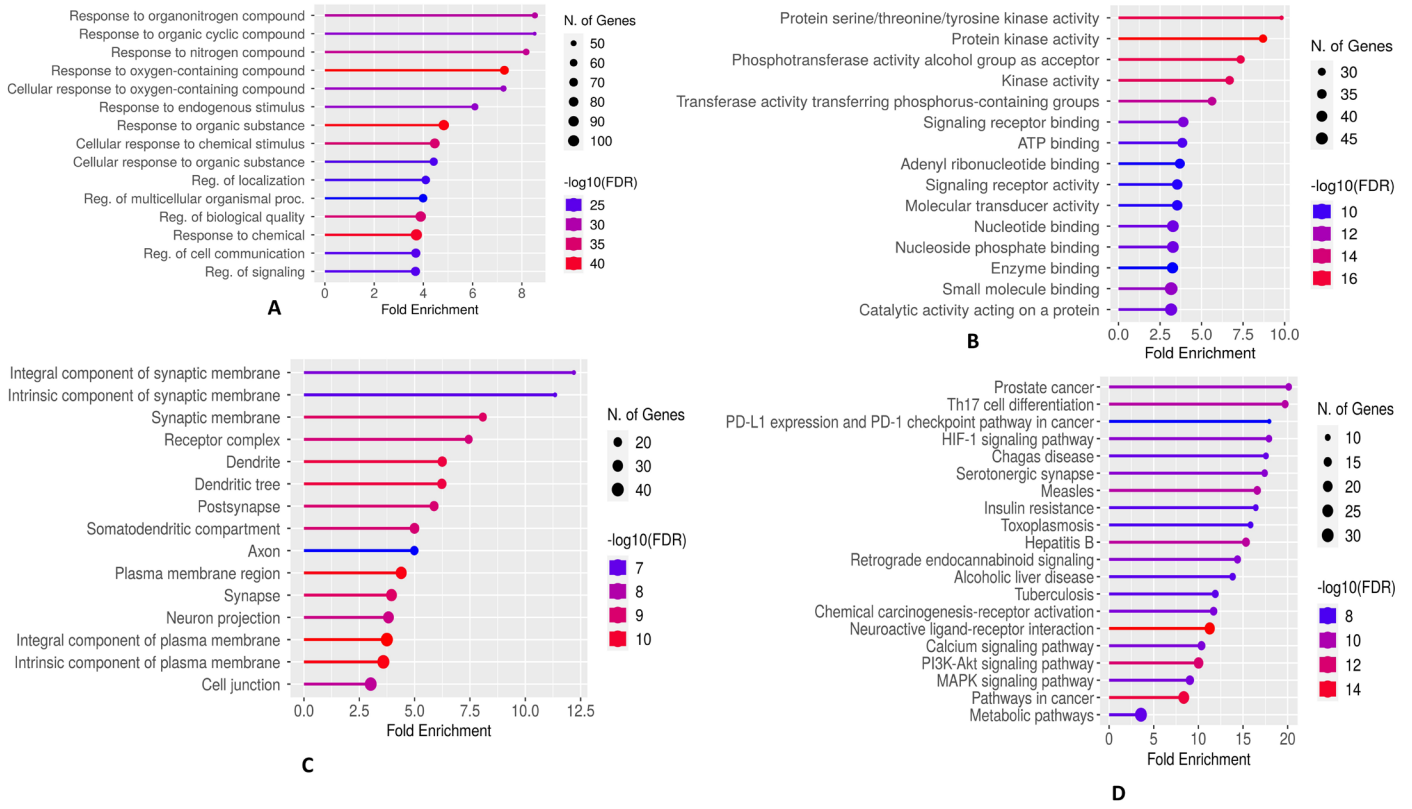

Figure 4: GO analysis of common targets using ShinyGO revealed significant (A) biological processes such as "Response to organonitrogen compound." (B) Key molecular functions included "Protein kinase activity," while (C) cellular component analysis identified "Synaptic membrane" and "Dendrite," suggesting roles in signaling and membrane-associated structures. (D) KEGG pathway analysis showed enrichment in PD-1/PD-L1 checkpoint pathway PI3K-Akt pathways and cancer pathways.

immune responses, cell signaling and various disease pathways. A gene mapping diagram was also obtained from the ShinyGo platform which depicted the targets of artemisinin enriched in cancer pathways (Figure 5A) and PI3K-Akt signaling pathway (Figure 5B). A network was constructed for the illustration of interactions between artemisinin, common targets and enriched pathways. The network showed 199 nodes and 519 edges with average number of neighbours of 5.2 (Figure 6).

DNA methylation, expression, proteomics and survival analysis

To further verify the active involvement of the identified hub targets, bioinformatic analyses were conducted using the UALCAN database, which provided insights into DNA methylation, gene expression, proteomics and survival outcomes of the hub genes in lung cancer. Results indicated that DNA methylation levels were elevated for EGFR and HSP90AA1, while HSP90AB1 showed lower methylation. NFKB1 and PTGS2 displayed no significant methylation changes (Figure 7).In terms of mRNA expression, HSP90AA1 and HSP90AB1 were upregulated, while EGFR, PTGS2 and NFKB1 showed downregulation, indicating differential gene expression trends across these targets in lung cancer (Figure 8).

Analysis of the proteomic expression profile (Z-values represent standard deviations from the median, normalized within and across samples) revealed that HSP90AA1 and HSP90AB1 protein levels were upregulated, while EGFR and NFKB1 were downregulated. No significant change in proteomics was observed for PTGS2, aligning with its stable methylation profile (Figure 9).

Survival analysis further demonstrated a downregulation in the expression of all hub genes except PTGS2, which maintained stable expression, suggesting a potential role for PTGS2 in lung cancer survival outcomes (Figure 10). These results emphasize distinct regulatory patterns of these genes, underscoring their potential as therapeutic targets in lung cancer.

Immune infiltration

To assess the relationship between hub genes and immune cell infiltration in lung cancer, TIMER, a comprehensive tool for immune infiltration analysis in cancer, was utilized. TIMER uses statistical methods to estimate the abundance of tumor-infiltrating immune cells, providing insights into how genetic variation and expression levels influence immune cell infiltration within tumor tissues. In this analysis, the top five hub genes (EGFR, HSP90AA1, PTGS1, HSP90AB1 and NFKB1) were examined for their correlation with tumor infiltration by the immune cells, a measure of the proportion of tumor cells in a sample relative to

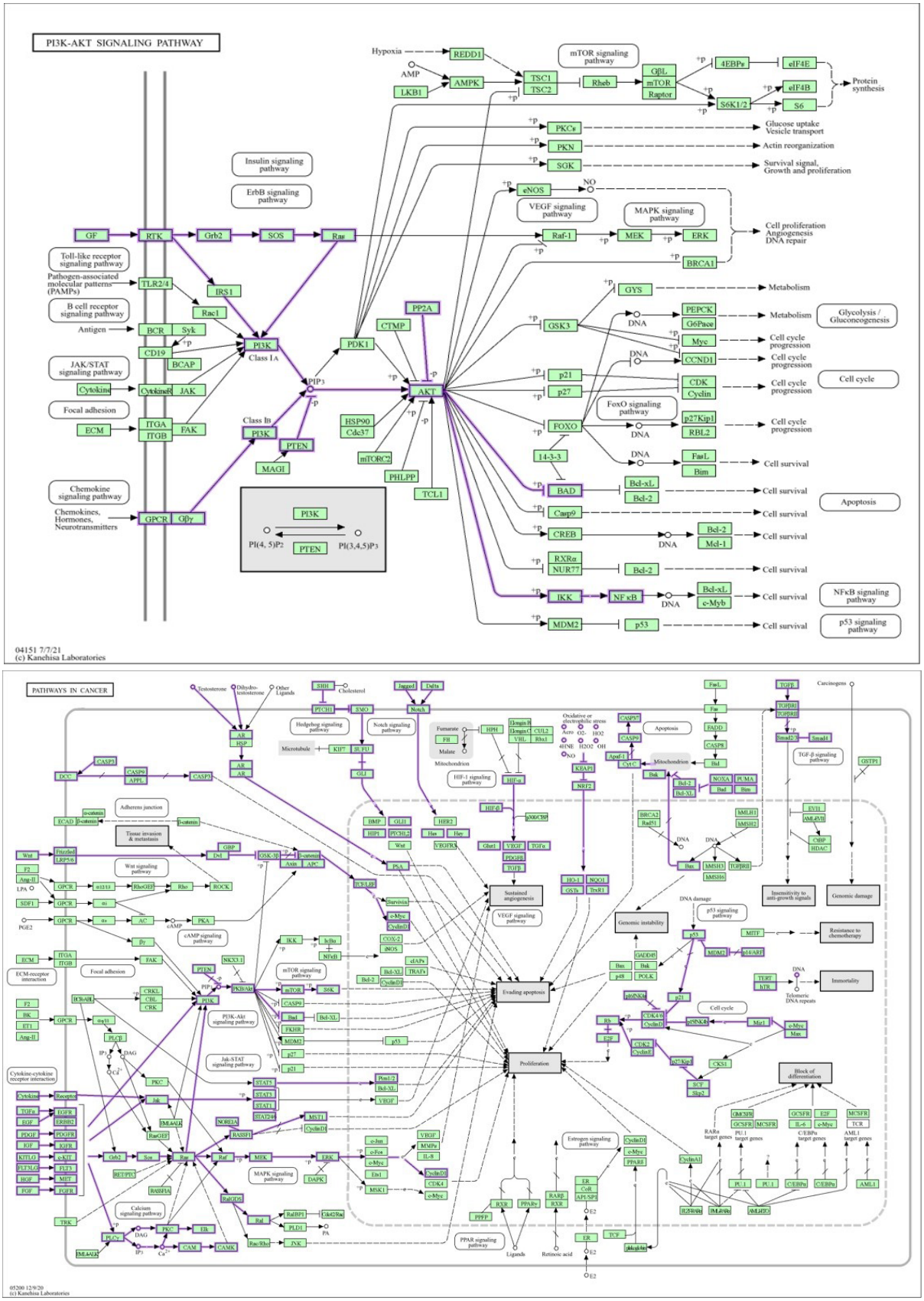

Figure 5: Gene mapping analysis from the ShinyGO platform illustrated the targets of (A) artemisinin enriched in cancer pathways and (B) highlighted their involvement in the PI3K-Akt signaling pathway.

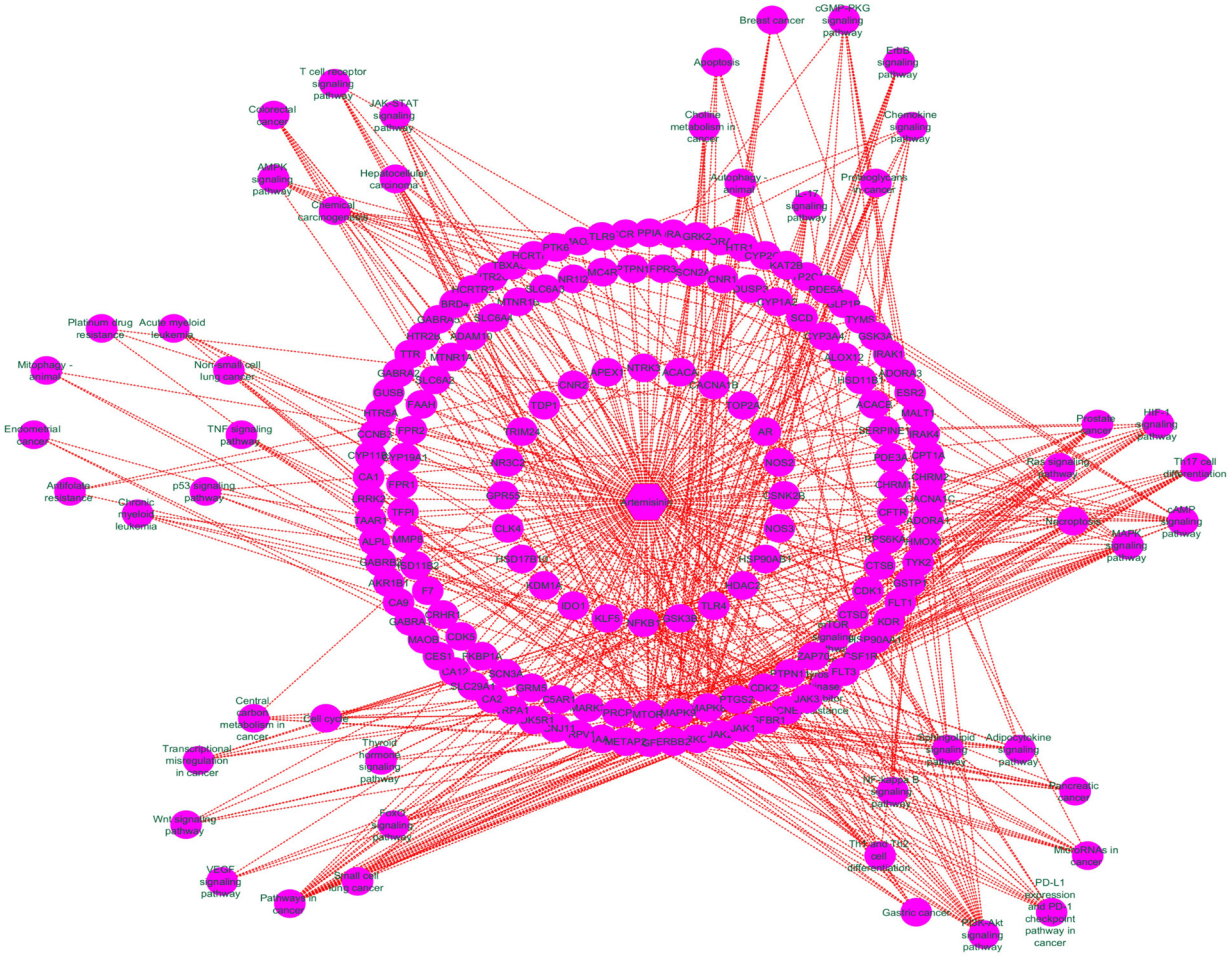

Figure 6: A comprehensive network illustrating interactions among artemisinin, common targets and enriched pathways was constructed, comprising 199 nodes and 519 edges, with an average neighbour count of 5.2. This network visualization highlights the complex relationships between artemisinin and its potential targets in cancer-related pathways.

Table 2: Molecular docking score for each of the artemisinin hub gene complex using CB-Dock2.

Complex	CurPocket ID	Vina score	Cavity volume (Å³)	Center (x, y, z)	Docking size (x, y, z)
Artemisinin-EGFR	C3	-8.1	303	0, -54, -23	18, 18, 18
Artemisinin-HSP90AA1	C1	-8.8	2154	7, 11, 25	26, 18, 18
Artemisinin-PTGS2	C2	-8.4	19357	48, 32, -2	35, 29, 33

The figures illustrate specific binding interactions: (A) artemisinin-EGFR bound to CurPocket C3 (-8.1 Vina score); (B) artemisinin-HSP90AA1 in CurPocket C1 (-8.8 Vina score); (C) artemisinin-PTGS2 in CurPocket C2 (-8.4 Vina score).

surrounding immune cells. Results demonstrated a significant positive correlation between these genes and tumor infiltration, as indicated by their respective p-values especially NFKB1 and EGFR (Figure 11). The results indicate that the expression of these hub genes may correlate with immune cell composition in the tumor microenvironment, providing significant perspectives for comprehending immunological interactions and therapeutic targeting in lung cancer.

Molecular Docking Interactions

A CB-Dock2 docking investigation of artemisinin with the hub genes EGFR, HSP90AA1 and PTGS2 revealed five potential active sites (CurPockets), which were further subjected to blind docking to assess binding interactions. All complexes exhibited elevated docking scores, suggesting advantageous binding (Table 2). Specifically, the artemisinin-EGFR complex bound to CurPocket C3 with a Vina score of -8.1 and a cavity volume of 303 Å³, with interacting residues in chain A including LEU718, GLY719, VAL726 and others (Figure 12A). For the

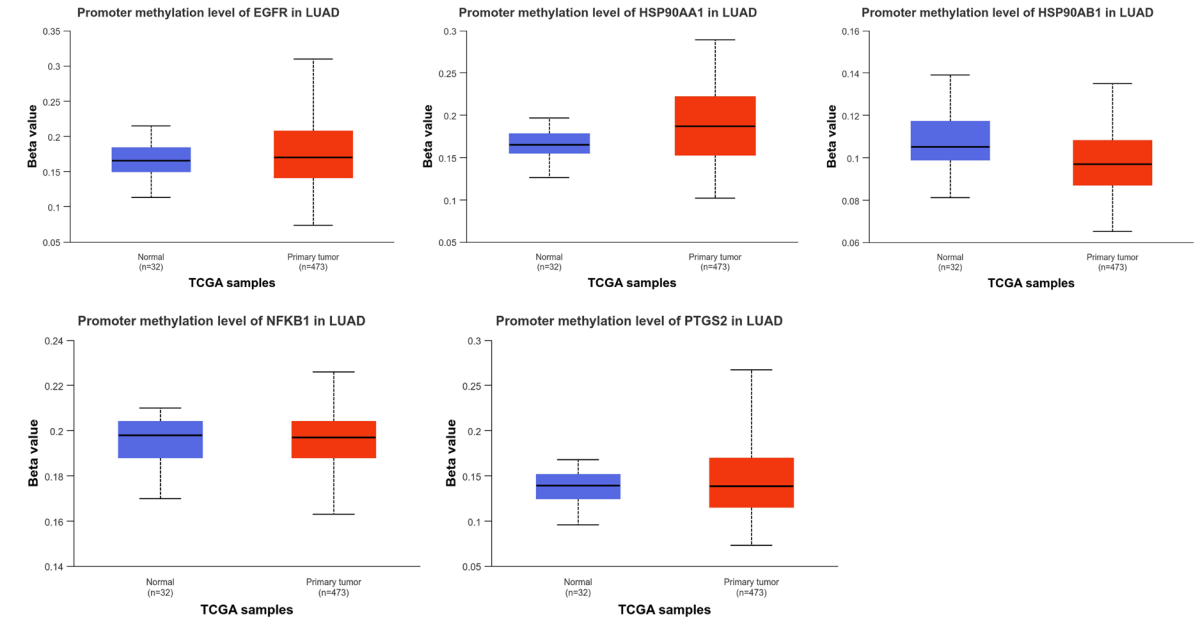

Figure 7: Bioinformatics analysis using the UALCAN database revealed elevated DNA methylation levels for EGFR and HSP90AA1, while HSP90AB1 exhibited lower methylation. NFKB1 and PTGS2 showed no significant methylation changes in lung cancer samples.

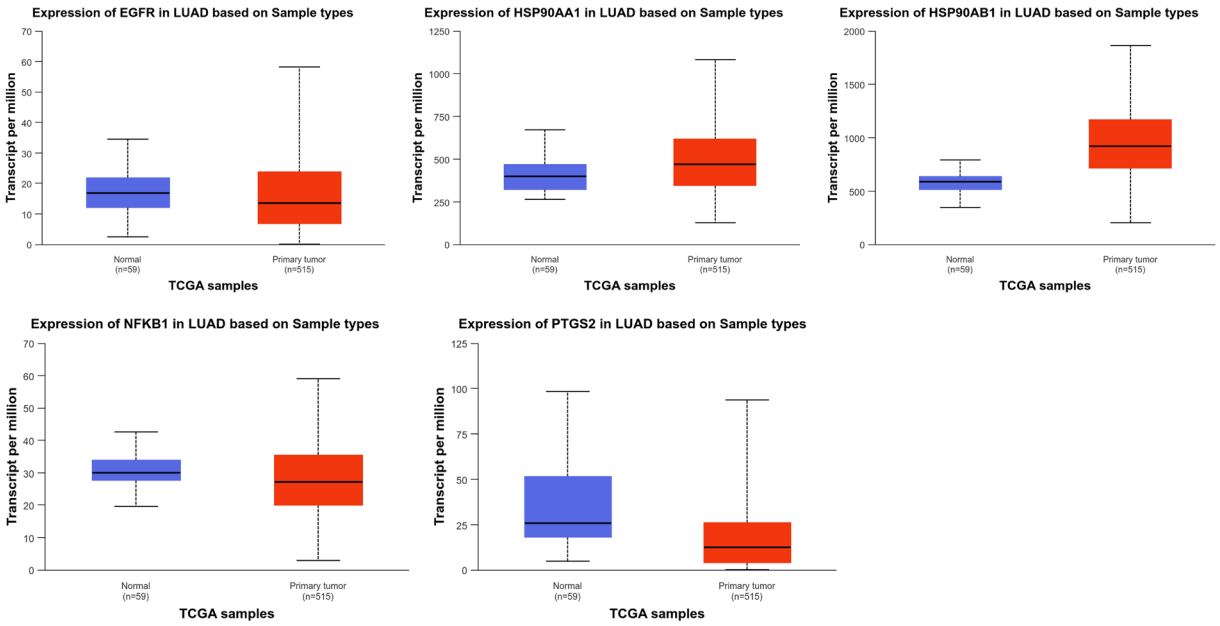

Figure 8: mRNA expression analysis indicated that HSP90AA1 and HSP90AB1 were upregulated, whereas EGFR, PTGS2 and NFKB1 displayed downregulation, highlighting differential expression patterns among these hub genes in lung cancer.

artemisinin-HSP90AA1 complex, the highest binding occurred in CurPocket C1 with a score of -8.8 and cavity volume of 2154 Å^3, involving residues such as ASN51, MET98 and TYR139 (Figure 12B). Artemisinin-PTGS2 showed strong binding in CurPocket C2 with a score of -8.4 and the largest cavity volume (19357 Å^3), involving multiple residues across chains A and B, such as TRP139 and LEU224 (Figure 12C). 2D interaction analysis using Discovery Studio revealed diverse interaction types, including van der Waals, alkyl, pi-alkyl, hydrogen bonds, pi-sigma and carbon-hydrogen bonds, underscoring the versatile binding of artemisinin to these proteins.

Molecular dynamics of the artemisinin docked hub gene complexes

CABS-flex 2.0 is a tool for simulating protein structure flexibility, efficiently using coarse-grained modelling to predict protein dynamics and residue fluctuation. With minimal computational resources, it provides accurate near-native dynamics and protein flexibility profiles. In the molecular dynamics simulations of artemisinin complexes with EGFR, HSP90AA1 and PTGS2, the RMSF results showed favourable binding stability, with low RMSF values indicating reduced residue flexibility across binding sites (Figure 13 A-C), supporting the stable interaction of artemisinin

with these proteins. Further, the contact map for each of the artemisinin complexes with EGFR, HSP90AA1 and PTGS2, were generated (Figure 13 A-C).

Artemisinin induced potent inhibition of cell viability in A-549 lung cancer cells

Artemisinin treatment caused a dose-dependent decrease in the viability of A549 cells. The viability was significantly decreased at higher doses (Figure 14A). However, the viability of normal L132 cells was not significantly affected, which is indicative of selective cytotoxicity towards lung cancer cells. In the colony assay, artemisinin revealed a significant decrease in the formation of colonies of A549; at higher concentrations, fewer and smaller colonies were observed, indicating strong antiproliferative activity and anticlonogenic potential (Figure 13B).

Artemisinin induced apoptosis

AO/EB staining revealed that the artemisinin-treated A549 cells had increased red fluorescence which indicated dose-dependent induction of apoptosis. Higher doses were associated with more cells expressing apoptotic characteristics, including chromatin condensation and membrane blebbing through the increase in red fluorescence (Figure 15A).

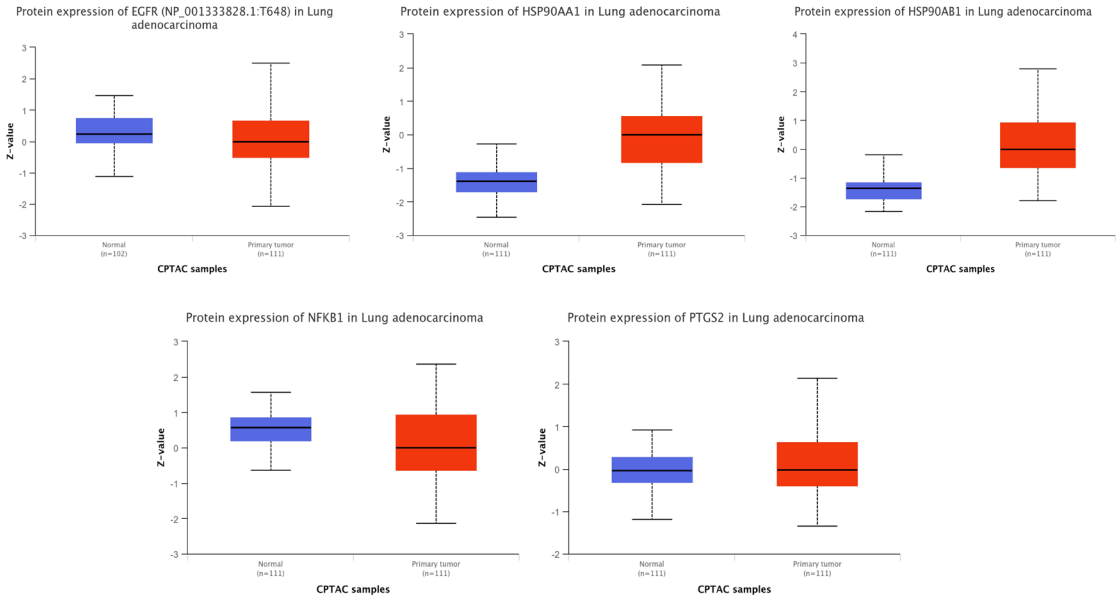

Figure 9: Proteomic expression profiles showed upregulation of HSP90AA1 and HSP90AB1 proteins, while EGFR and NFKB1 were downregulated; PTGS2 exhibited stable proteomic expression consistent with its methylation profile.

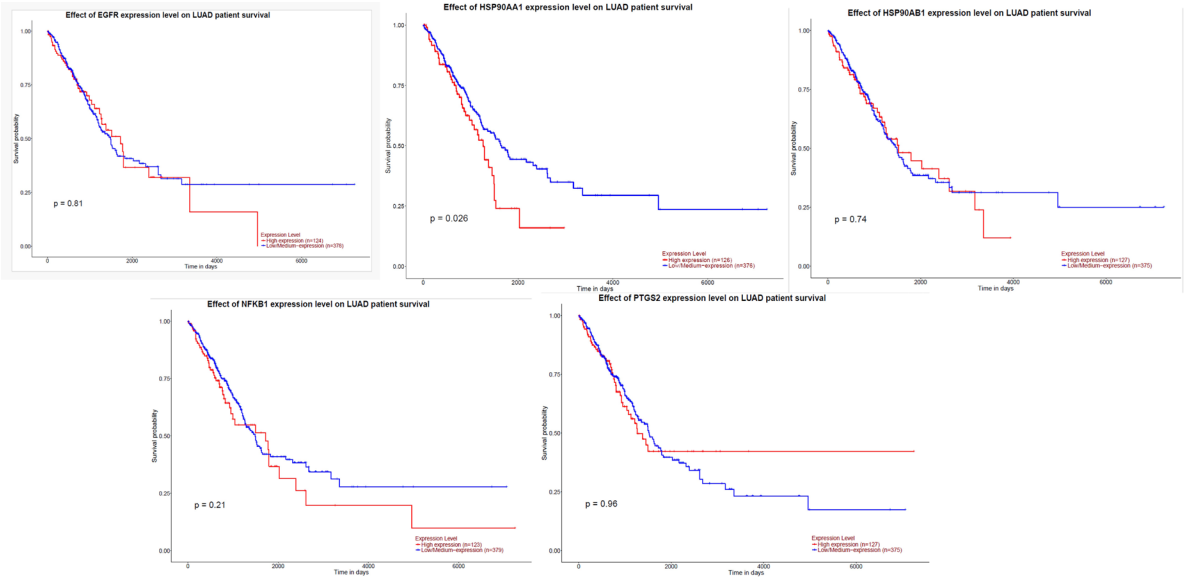

Figure 10: Survival analysis demonstrated that all hub genes, except PTGS2, were downregulated, suggesting PTGS2's stable expression may play a role in improved survival outcomes in lung cancer patients.

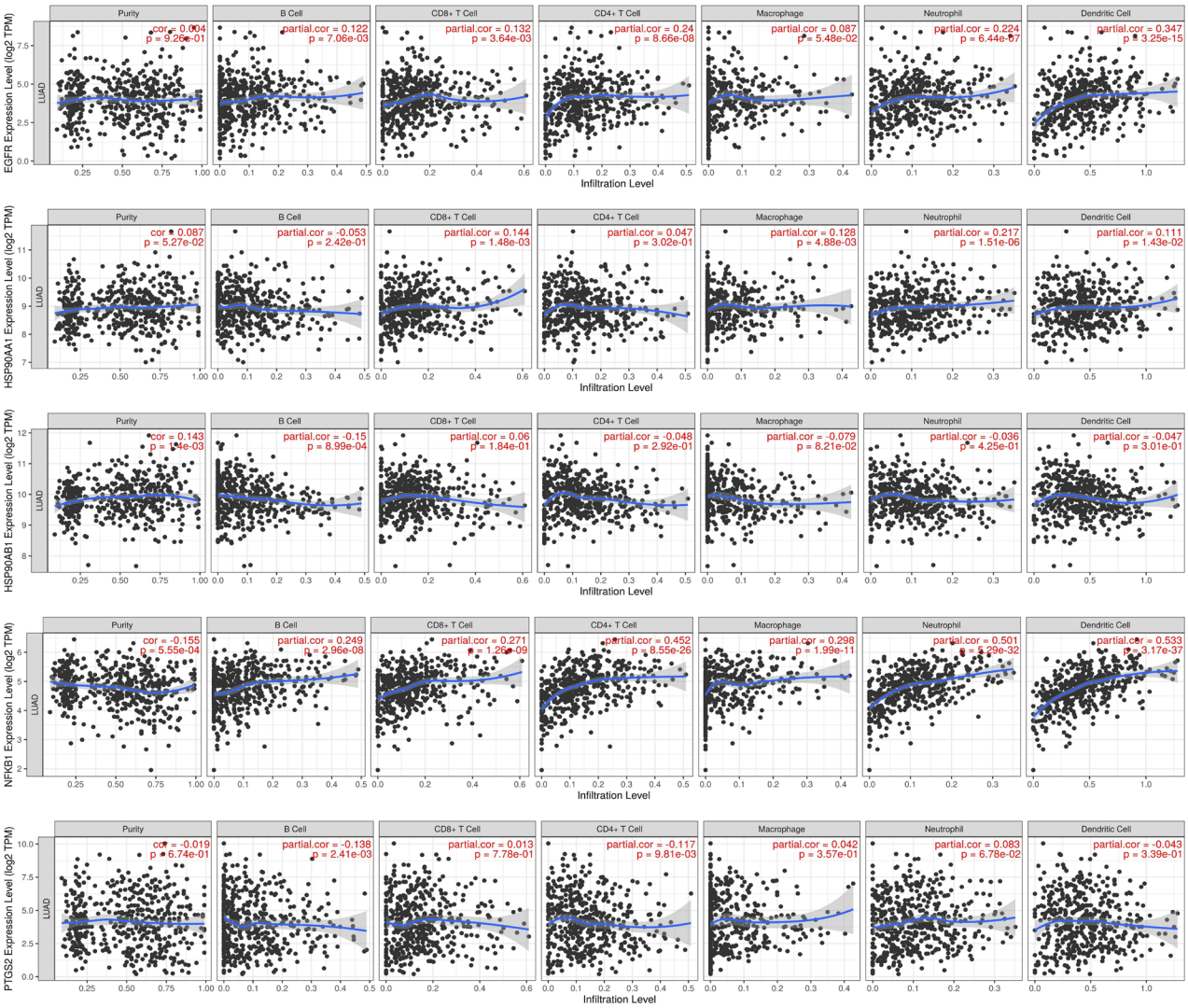

Figure 11: Using TIMER, the correlation between hub genes (EGFR, HSP90AA1, PTGS1, HSP90AB1 and NFKB1) and tumor infiltration by various immune cells in lung cancer was assessed. The analysis revealed a significant positive correlation between hub gene expression and tumor infiltration level especially NFKB1 and EGFR, suggesting that their expression may influence immune cell composition within the tumor microenvironment.

Artemisinin downregulated the expression of hub genes

Western blotting analysis of artemisinin treated A549 cells displayed dose dependent down regulation of the proteins EGFR, HSP90AA1 and PTGS2 (Figure 15B). Figure 15C demonstrate the graphical representation of the relative expressions of hub genes in treated and control A549 cells. The results showed that all three over-expressed hub genes in untreated group were significantly downregulated in treatment group. The downregulation in hub gene expressions showed dose dependence to artemisinin concentrations. Therefore, artemisinin may inhibit pathways important to the survival and growth of cancerous cells by targeting these oncogenic proteins.

DISCUSSION

Lung cancer is one of the leading causes of cancer mortality worldwide, largely due to its aggressive nature, high incidence rates and frequent diagnosis at advanced stages.[1,2] The flaws in current treatment options compel to explore new avenues, like network pharmacology and natural compounds, to improve therapeutic outcomes and patient survival.

Network pharmacology, a powerful tool for mapping drug-target interactions, reveals that artemisinin targets 138 overlapping genes associated with lung cancer, highlighting its multifunctional potential in modulating cancer-relevant pathways.[21] Using PPI network, Cytoscape analysis identified 10 principal hub genes, including EGFR, HSP90AA1, PTGS2, NFKB1 and HSP90AB1. The discovery of these hub genes inside the network indicates their pivotal involvement in cancer-related pathways. Cancer and lung

cancer in particular, is known to interact with EGFR, HSP90AA1, PTGS2, HSP90AB1 and NFKB1-through proliferation, survival, inflammation and immunological pathways. The EGFR is key to the proliferation of cancer cells and overexpressed in lung cancer and is therefore a very important therapeutic target.[22,23] HSP90AA1 is a stress protein involved in the stability and functions of several oncogenic proteins and its inhibition had been shown to impair viability of cancer cells.[24] PTGS2, also called COX-2, promotes inflammation and is connected with carcinogenesis.[25] The same way, HSP90AB1 contributes towards the stability of proteins taking part in cell signalling and death and NFKB1 governs responses of immunological and inflammatory, which are critical factors in carcinogenesis and in the growth of tumors.[26,27] With an emphasis on the regulation at various levels of these genes by artemisinin, this compound could represent a potential strategy for targeting cancer growth.

Functional enrichment study confirmed that these genes participate in essential biological processes, including "Protein kinase activity," "ATP binding," and cellular signalling pathways, aligning with their functions in cancer signalling and proliferation. KEGG pathway analysis indicated their participation in essential cancer pathways, such as PI3K-Akt and PD-L1/PD-1, both pivotal in cancer proliferation and immune evasion, demonstrating impact of artemisinin on pathways critical to tumour survival and development.[28,29]

The DNA methylation and gene expression analyses using UALCAN database revealed distinct methylation and expression patterns of these hub genes in lung cancer, with EGFR and HSP90AA1 exhibiting elevated DNA methylation. The UALCAN database is a comprehensive and user-friendly web resource for Analyzing cancer transcriptomics data from The Cancer Genome Atlas (TCGA) and other sources. It allows researchers to explore gene expression profiles across various cancer types, stages and patient subgroups based on clinical attributes such as race, age, or tumor grade. The differential expression patterns of these genes indicate that impact of artemisinin on lung cancer may be mediated by modifications in gene expression at the epigenetic level. Proteomic analysis corroborated these results, revealing elevation of HSP90AA1 and HSP90AB1, whereas EGFR and NFKB1 exhibited downregulation, therefore strengthening the evidence of the potential influence of artemisinin on protein expression and stability in cancer cells. The steady expression of PTGS2 indicates its potential consistent function in cancer pathways,

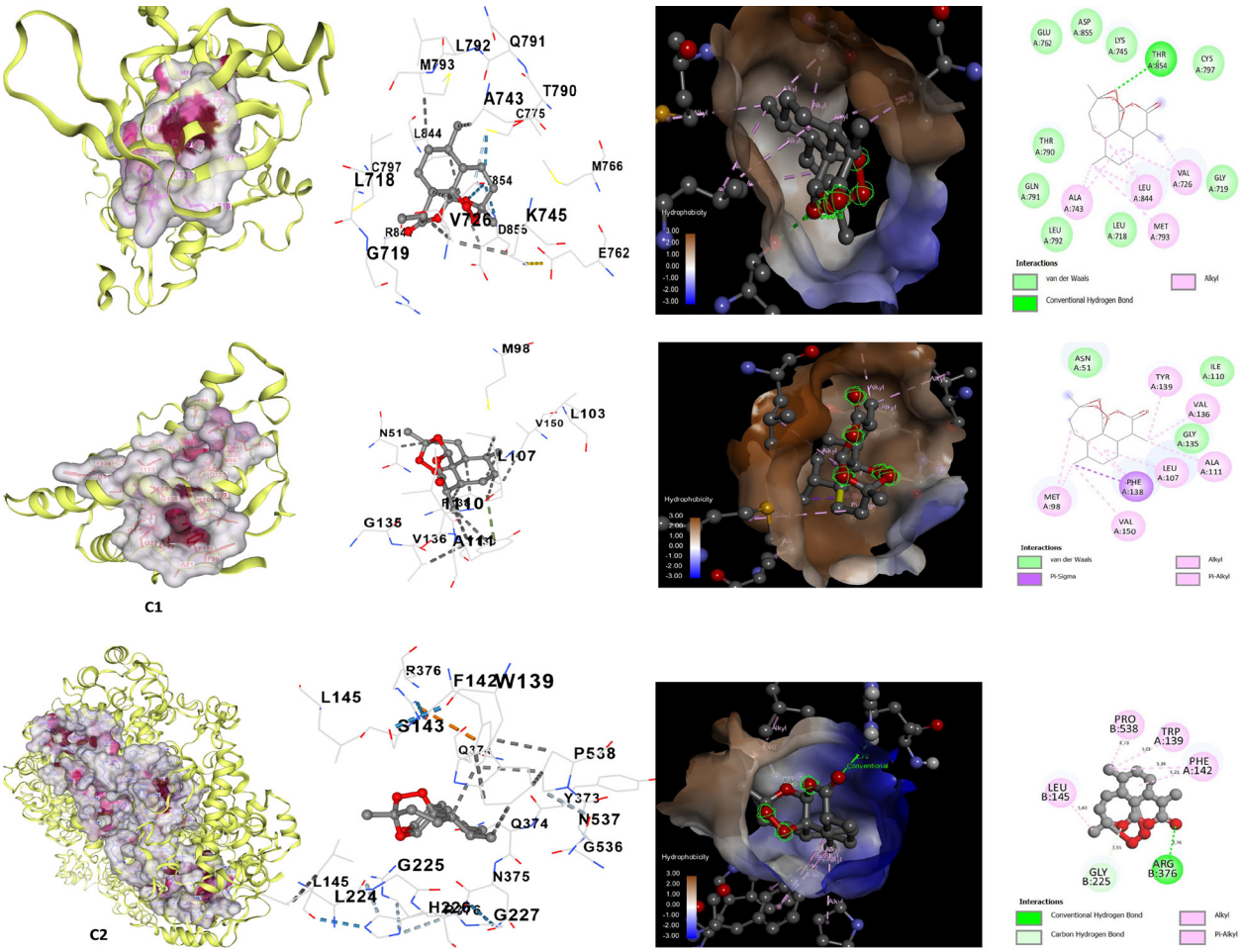

Figure 12: Molecular docking analysis using CB-Dock2 identified 5 potential active sites (CurPockets) for artemisinin in complexes with hub genes EGFR, HSP90AA1 and PTGS2.

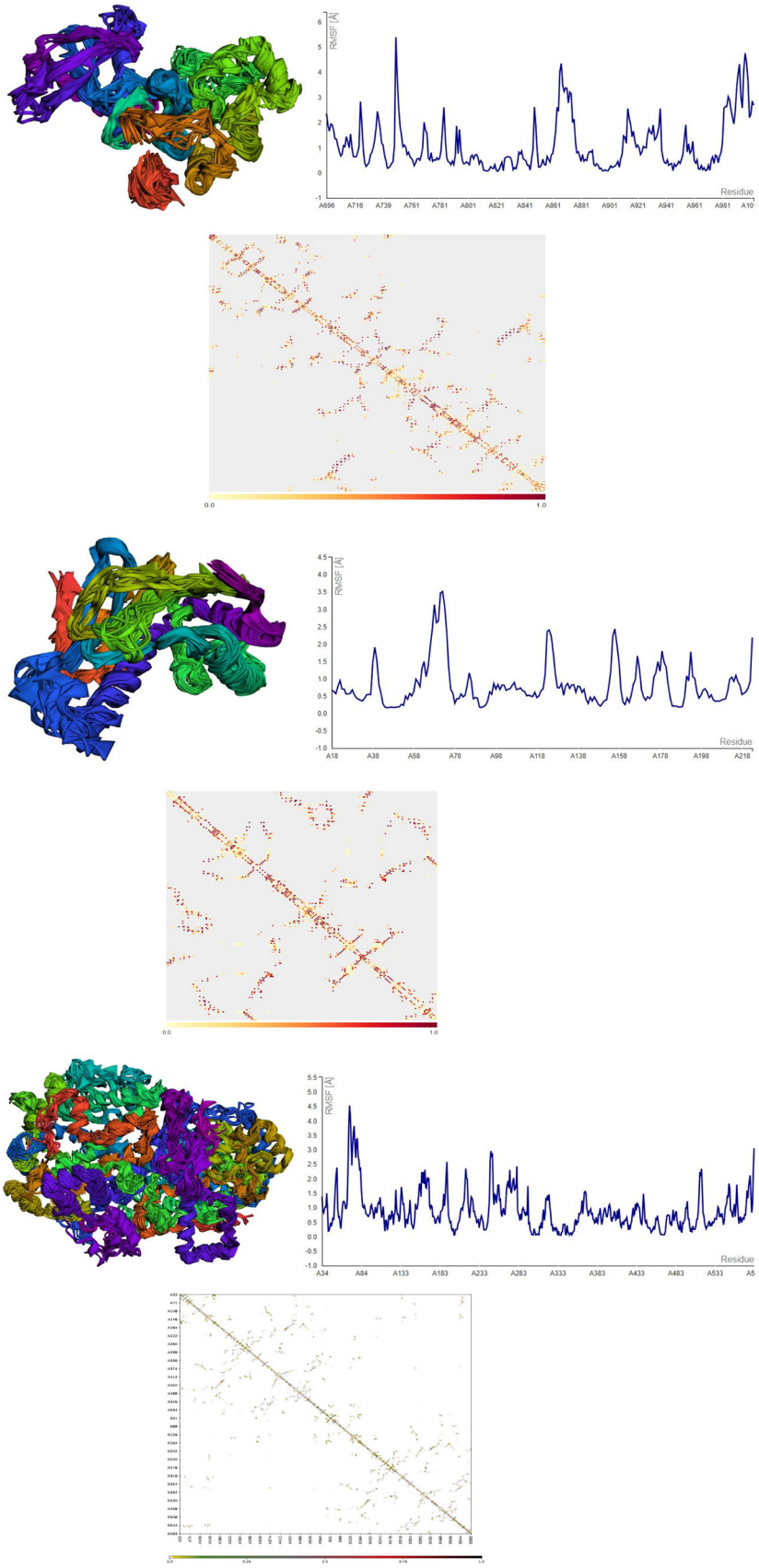

Figure 13: Molecular dynamics simulations of artemisinin complexes with (A) EGFR, (B) HSP90AA1 and (C) PTGS2 were performed using CABS-flex 2.0, revealing favourable binding stability indicated by low RMSF values across the binding sites. Contact maps generated for each complex provide additional insights into residue interactions, supporting the stability of artemisinin's binding to these proteins.

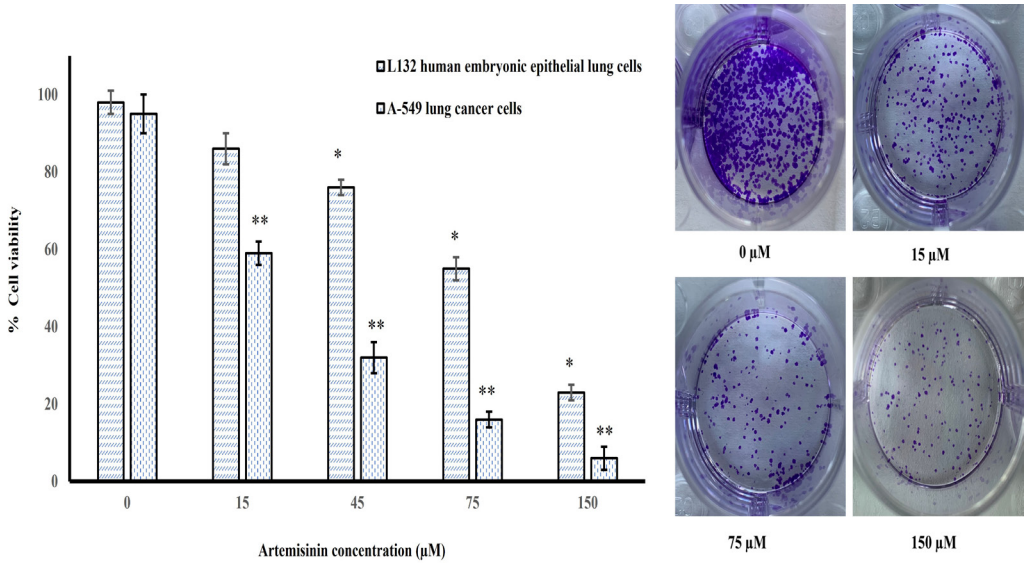

Figure 14: Viability inhibition (A) Artemisinin induces dose dependent cytotoxic inhibition of A549 cells significant in comparison to control group after 24 hr of treatment. (B) The anti-clonogenic properties of artemisinin are shown by the clonogenic test, which reveals a decreased number of blue stains with increasing concentration indicating colony inhibition.

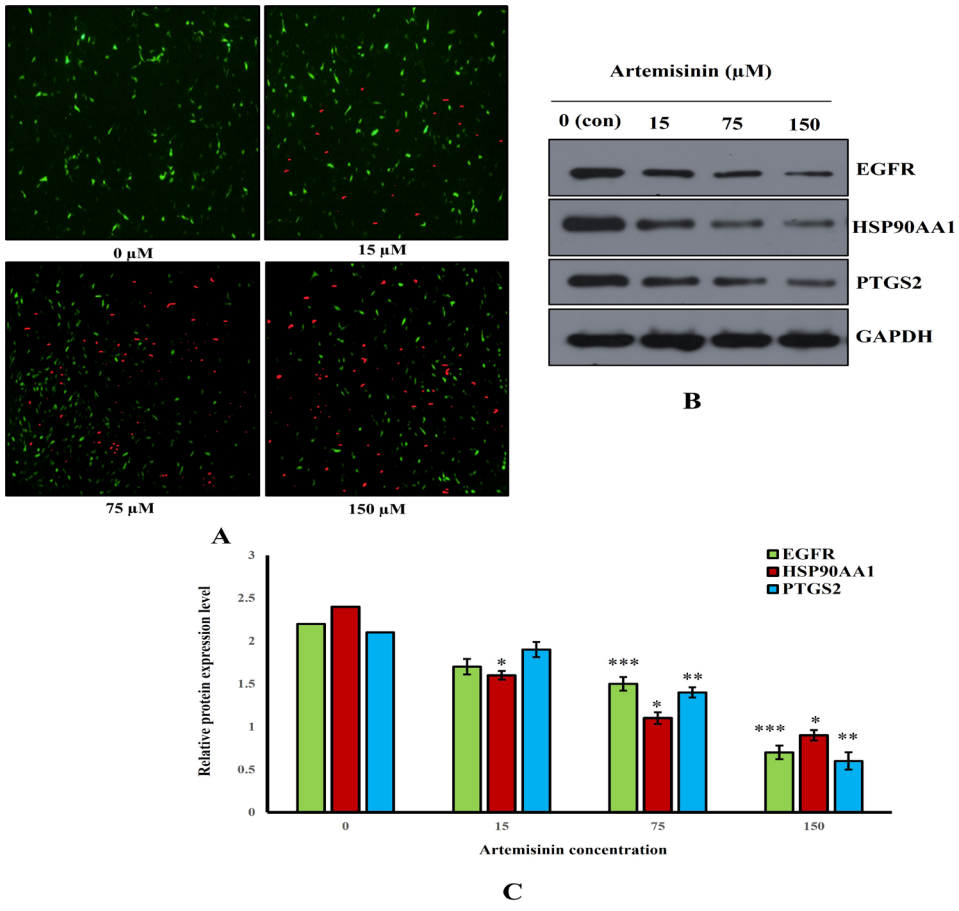

Figure 15: (A) Acridine Orange/Ethidium Bromide (AO/EB) staining of A549 cells treated with artemisinin at increasing concentrations, demonstrating dose-dependent apoptosis. Red fluorescence marks apoptotic cells with chromatin condensation and membrane blebbing, which intensifies at higher artemisinin doses. (B) Western blot analysis showing the downregulation of EGFR, HSP90AA1 and PTGS2 proteins in response to artemisinin in a dose-dependent manner. (C) Summary of Western blot findings, highlighting that artemisinin disrupts oncogenic pathways essential for cancer cell survival. GADPH served as a loading control, confirming consistent protein expression across samples.

as corroborated by survival studies, indicating importance of PTGS2 in cancer development.[30]

The TIMER analysis revealed substantial correlations between the identified hub genes and immune cell infiltration in lung cancer tissues, especially concerning tumour purity. The published data suggest that artemisinin may influence the immunological dynamics within the tumor microenvironment, a valuable attribute for therapeutic intervention. Artemisinin could enhance anti-tumor immune responses by potentially altering the immune microenvironment within tumors, thereby increasing its therapeutic potential in lung cancer.[31]

Molecular docking and dynamics simulations elucidated the connections between artemisinin and the hub proteins, revealing elevated docking scores that signify stronger binding affinities. Artemisinin had the most binding affinity to HSP90AA1 at CurPocket C1, emphasising its ability for stable and flexible interactions across several binding sites. The variety of interactions, including van der Waals forces and hydrogen bonds, illustrates flexible binding characteristics of artemisinin, essential for therapeutic effectiveness. Molecular dynamics simulations confirmed the durability of these interactions, as seen by low RMSF values at binding sites, suggesting strong binding stability and corroborating the steady interaction of artemisinin with these cancer-associated proteins.

Artemisinin demonstrates dose-dependent cytotoxicity and effectively promotes apoptosis in A549 lung cancer cells, as shown by MTT, colony formation and AO/EB staining tests. Natural products have long been regarded as promising therapeutic agents, especially in oncology, due to their ability to induce apoptosis and inhibit cancer cell growth.[32,33] Thus, our study suggests that artemisinin induces apoptosis-driven anticancer effects in A549 cells, highlighting its potential as a natural product-based therapeutic option for lung cancer treatment.

Validation of the hub genes EGFR, HSP90AA1 and PTGS2 in lung cancer was performed to confirm their differential expression in A549 cells. Using Western blotting, we observed that these genes, known to be implicated in tumor progression, displayed altered protein expression levels in artemisinin-treated A549 cells. Specifically, EGFR and HSP90AA1, which are involved in cell proliferation and stress response, showed significant downregulation, confirming their roles in lung cancer survival pathways. PTGS2, a key player in inflammation and carcinogenesis, also exhibited reduced expression following artemisinin treatment. These findings align with bioinformatic predictions and support their involvement in lung cancer progression, validating their status as therapeutic targets.

CONCLUSION

Artemisinin shows promising anticancer properties in lung cancer cells under *in vitro* conditions. Network analysis revealed 138 intersecting genes, with hub genes EGFR, HSP90AA1, PTGS2, HSP90AB1 and NFKB1 playing key roles in cancer pathways. Gene ontology highlighted crucial biological processes, while KEGG pathway analysis showed artemisinin targets cancer-related pathways. UALCAN analysis noted specific methylation and expression patterns of hub genes and TIMER results linked hub genes to immune infiltration. Docking studies confirmed strong binding affinities. MTT, clonogenic and AO/EB staining assays showed artemisinin's dose-dependent cytotoxicity and apoptosis in A549 cells. Western blotting confirmed downregulation of EGFR, HSP90AA1 and PTGS2, aligning with bioinformatics findings.

CONFLICT OF INTEREST

The authors declare that there is no conflict of interest.

ABBREVIATIONS

PPI: Protein-Protein Interactions; **KEGG:** Kyoto Encyclopedia of Genes and Genomes; **GO:** Gene Ontology; **UALCAN:** The University of ALabama at Birmingham CANcer data analysis Portal; **MTT:** 3-(4,5-dimethylthiazol-2-yl)-2,5-diphenyltetrazolium bromide; **AO/EB:** Acridine Orange/Ethidium Bromide; **NSCLC:** Non-Small Cell Lung Cancer; **SCLC:** Small Cell Lung Cancer; **BBB:** Blood-Brain Barrier; **DMSO:** Dimethyl Sulfoxide; **BCA:** Bicinchoninic Acid.

SUMMARY

Artemisinin shows promise as an anticancer agent against lung cancer, though its precise mechanisms of action require clarification. This study combines network pharmacology, bioinformatics, molecular docking, molecular dynamics simulations and *in vitro* experiments to investigate the anticancer effects of artemisinin. Using tools like SwissADME and Protox-II, the study confirmed artemisinin's favorable physiochemical and toxicity profiles. Target genes of artemisinin and lung cancer were identified and overlapped, generating a Protein-Protein Interaction (PPI) network of 137 nodes and 858 edges with 10 key hub genes, including EGFR, HSP90AA1 and PTGS2. Functional analyses highlighted pathways such as PD-L1 expression and PI3K-Akt signaling, with UALCAN data showing high DNA methylation levels in EGFR and HSP90AA1 and elevated expression of HSP90AA1 and HSP90AB1. Immune infiltration analysis found correlations between hub gene expression (e.g., NFKB1 and EGFR) and tumor immune infiltration. Molecular docking demonstrated strong binding affinities between artemisinin and key genes, while molecular dynamics confirmed stable interactions. Experimental assays showed artemisinin's dose-dependent cytotoxicity in A549 lung cancer cells, inducing

apoptosis and downregulating EGFR, PTGS2 and HSP90AA1. The findings support artemisinin's therapeutic potential in lung cancer and suggest future research directions targeting these pathways.

REFERENCES

1. Thandra KC, Barsouk A, Saginala K, Aluru JS, Barsouk A. Epidemiology of lung cancer. Contemp Oncol (Pozn). 2021; 25(1): 45-52. doi: 10.5114/wo.2021.103829, PMID 33911981.
2. Siegel RL, Giaquinto AN, Jemal A. Cancer statistics, 2024. CA Cancer J Clin. 2024; 74(1): 12-49. doi: 10.3322/caac.21820, PMID 38230766.
3. Garinet S, Wang P, Mansuet-Lupo A, Fournel L, Wislez M, Blons H. Updated prognostic factors in localized NSCLC. Cancers. 2022; 14(6): 1400. doi: 10.3390/cancers14061400, PMID 35326552.
4. Asmara OD, Hardavella G, Ramella S, Petersen RH, Tietzova I, Boerma EC, *et al.* Stage III NSCLC treatment options: too many choices. Breathe (Sheff). 2024; 20(3): 240047. doi: 10.1183/20734735.0047-2024, PMID 39360027.
5. Kesri R, Goyal H, Gupta G, Bharti D, Sharma R. Prevalence and clinicopathologic risk factors for epidermal growth factor receptor, anaplastic lymphoma kinase and ROS-1 fusion in metastatic non-small cell lung carcinoma. J Radiat Cancer Res. 2022; 13(2): 48-53. doi: 10.4103/jrcr.jrcr_43_21.
6. Kishore RR, Pan V. Correlation between ALK, ROS1 biomarkers and EGFR oncogene mutations in lung tumours: our observations in an apex oncopathology laboratory. Asian Pac J Cancer Biol. 2023; 8(2): 111-7. doi: 10.31557/apjcb.2023.8.2.111-117.
7. Qamar F, Ashrafi K, Singh A, Dash PK, Abdin MZ. Artemisinin production strategies for industrial scale: current progress and future directions. Ind Crops Prod. 2024; 218: 118937. doi: 10.1016/j.indcrop.2024.118937.
8. Khanal P. Antimalarial and anticancer properties of artesunate and other artemisinins: current development. Monatsh Chem. 2021; 152(4): 387-400. doi: 10.1007/s00706-021-02759-x, PMID 33814617.
9. Tsamesidis I, Pério P, Pantaleo A, Reybier K. Oxidation of erythrocytes enhance the production of reactive species in the presence of artemisinins. Int J Mol Sci. 2020; 21(13): 4799. doi: 10.3390/ijms21134799, PMID 32646002.
10. Li R, Li Y, Liang X, Yang L, Su M, Lai KP. Network Pharmacology and bioinformatics analyses identify intersection genes of niacin and COVID-19 as potential therapeutic targets. Brief Bioinform. 2021; 22(2): 1279-90. doi: 10.1093/bib/bbaa300, PMID 33169132.
11. Rathaur P, Soni MN, Gelat B, Rawal R, Pandya HA, Johar K. Network pharmacology-based evaluation of natural compounds with paclitaxel for the treatment of metastatic breast cancer. Toxicol Appl Pharmacol. 2021; 423: 115576. doi: 10.1016/j.taap.2021.115576, PMID 34000264.
12. Madeddu C, Donisi C, Liscia N, Lai E, Scartozzi M, Macciò A. EGFR-mutated non-small cell lung cancer and resistance to immunotherapy: role of the tumor microenvironment. Int J Mol Sci. 2022; 23(12): 6489. doi: 10.3390/ijms23126489, PMID 35742933.
13. Zhang A, Miao K, Sun H, Deng CX. Tumor heterogeneity reshapes the tumor microenvironment to influence drug resistance. Int J Biol Sci. 2022; 18(7): 3019-33. doi: 10.7150/ijbs.72534, PMID 35541919.
14. Daina A, Michielin O, Zoete V. SwissADME: a free web tool to evaluate pharmacokinetics, drug-likeness and medicinal chemistry friendliness of small molecules. Sci Rep. 2017; 7(1): 42717. doi: 10.1038/srep42717, PMID 28256516.
15. Daina A, Michielin O, Zoete V. SwissTargetPrediction: updated data and new features for efficient prediction of protein targets of small molecules. Nucleic Acids Res. 2019; 47(W1):W357-64. doi: 10.1093/nar/gkz382, PMID 31106366.
16. Szklarczyk D, Kirsch R, Koutrouli M, Nastou K, Mehryary F, Hachilif R, *et al.* The STRING database in 2023: protein-protein association networks and functional enrichment analyses for any sequenced genome of interest. Nucleic Acids Res. 2023; 51(D1):D638-46. doi: 10.1093/nar/gkac1000, PMID 36370105.
17. Chandrashekar DS, Karthikeyan SK, Korla PK, Patel H, Shovon AR, Athar M, *et al.* UALCAN: an update to the integrated cancer data analysis platform. Neoplasia. 2022; 25: 18-27. doi: 10.1016/j.neo.2022.01.001, PMID 35078134.
18. Li T, Fu J, Zeng Z, Cohen D, Li J, Chen Q, *et al.* TIMER2. 0 for analysis of tumor-infiltrating immune cells. Nucleic Acids Res. 2020; 48(W1):W509-14. doi: 10.1093/nar/gkaa407, PMID 32442275.
19. Liu Y, Yang X, Gan J, Chen S, Xiao ZX, Cao Y. CB-Dock2: improved protein-ligand blind docking by integrating cavity detection, docking and homologous template fitting. Nucleic Acids Res. 2022; 50(W1):W159-64. doi: 10.1093/nar/gkac394, PMID 35609983.
20. Kuriata A, Gierut AM, Oleniecki T, Ciemny MP, Kolinski A, Kurcinski M, *et al.* CABS-flex 2.0: a web server for fast simulations of flexibility of protein structures. Nucleic Acids Res. 2018; 46(W1):W338-43. doi: 10.1093/nar/gky356, PMID 29762700.
21. Nogales C, Mamdouh ZM, List M, Kiel C, Casas AI, Schmidt HH. Network pharmacology: curing causal mechanisms instead of treating symptoms. Trends Pharmacol Sci. 2022; 43(2): 136-50. doi: 10.1016/j.tips.2021.11.004, PMID 34895945.
22. Passaro A, Jänne PA, Mok T, Peters S. Overcoming therapy resistance in EGFR-mutant lung cancer. Nat Cancer. 2021; 2(4): 377-91. doi: 10.1038/s43018-021-00195-8, PMID 35122001.
23. To KK, Fong W, Cho WC. Immunotherapy in treating EGFR-mutant lung cancer: current challenges and new strategies. Front Oncol. 2021; 11: 635007. doi: 10.3389/fonc.2021.635007, PMID 34113560.
24. Bhattacharyya N, Gupta S, Sharma S, Soni A, Bagabir SA, Bhattacharyya M, *et al.* CDK1 and HSP90AA1 appear as the novel regulatory genes in non-small cell lung cancer: a bioinformatics approach. J Pers Med. 2022; 12(3): 393. doi: 10.3390/jpm12030393, PMID 35330393.
25. Liang X, Wang J, Liu Y, Wei L, Tian F, Sun J, *et al.* Polymorphisms of COX/PEG2 pathway-related genes are associated with the risk of lung cancer: a case-control study in China. Int Immunopharmacol. 2022; 108: 108763. doi: 10.1016/j.intimp.2022.108763, PMID 35430434.
26. Lin X, Liu YH, Zhang HQ, Wu LW, Li Q, Deng J, *et al.* DSCC1 interacts with HSP90AB1 and promotes the progression of lung adenocarcinoma via regulating ER stress. Cancer Cell Int. 2023; 23(1): 208. doi: 10.1186/s12935-023-03047-w, PMID 37742009.
27. Rasmi RR, Sakthivel KM, Guruvayoorappan C. NF-κB inhibitors in treatment and prevention of lung cancer. Biomed Pharmacother. 2020; 130: 110569. doi: 10.1016/j.biopha.2020.110569, PMID 32750649.
28. Zhou S, Wang B, Wei Y, Dai P, Chen Y, Xiao Y, *et al.* Yin W. PD-1 inhibitor combined with docetaxel exerts synergistic antiprostate cancer effect in mice by down-regulating the expression of PI3K/AKT/NFKB-P65/PD-L1 signaling pathway. Cancer Biomark. 2024: 1-13.
29. Han Y, Liu D, Li L. PD-1/PD-L1 pathway: current researches in cancer. Am J Cancer Res. 2020; 10(3): 727-42. PMID 32266087.
30. Kamal MV, Damerla RR, Parida P, Rao M, Belle VS, Dikhit PS, *et al.* Expression of PTGS2 along with genes regulating VEGF signalling pathway and association with high-risk factors in locally advanced oral squamous cell carcinoma. Cancer Med. 2024; 13(3): e6986. doi: 10.1002/cam4.6986, PMID 38426619.
31. Rangamuwa K, Aloe C, Christie M, Asselin-Labat ML, Batey D, Irving L, *et al.* Methods for assessment of the tumour microenvironment and immune interactions in non-small cell lung cancer. A narrative review. Front Oncol. 2023; 13: 1129195. doi: 10.3389/fonc.2023.1129195, PMID 37143952.
32. Huang M, Lu JJ, Ding J. Natural products in cancer therapy: past, present and future. Nat Prod Bioprospect. 2021; 11(1): 5-13. doi: 10.1007/s13659-020-00293-7, PMID 33389713.
33. Mosca L, Ilari A, Fazi F, Assaraf YG, Colotti G. Taxanes in cancer treatment: activity, chemoresistance and its overcoming. Drug Resist Updat. 2021; 54: 100742. doi: 10.1016/j.drup.2020.100742, PMID 33429249.

Cite this article: Sheng X, Sheng D, Xing R. Deciphering Key Protein Targets, Hub Gene Networks, Signaling Pathways and *in silico* Docking Studies of Artemisinin in Human Lung Carcinoma. Indian J of Pharmaceutical Education and Research. 2026;60(1):393-409.